Forecasting Research

Forecasting Research Division
Technical Report No. 44

A REVIEW OF SEA ICE MODELS FOR USE IN FOAM

by

C G Sherlock

April 1993

Meteorological Office
London Road
Bracknell
Berkshire
RG12 2SZ
United Kingdom

Forecasting Research Division
Technical Report No 44

A REVIEW OF SEA ICE MODELS FOR USE IN FOAM

by

C G Sherlock

April 1993

Forecasting Research Division
Meteorological Office
London Road
Bracknell
Berkshire RG12 2SZ
ENGLAND

N.B. This paper has not been published. Permission to quote from it must be obtained from the above Met. Office division.

ABSTRACT

This report examines several numerical models of sea ice, which have been developed at various research centres, to determine their suitability for use within the Meteorological Office Forecasting Ocean Atmosphere Model (FOAM). A review of the basic concepts involved in the dynamic and thermodynamic modelling of sea ice provides the platform for the discussion of the models themselves.

Heat fluxes across the air/ice and ice/ocean interfaces are described, and salinity changes within the ice and ocean are mentioned. The components of the sea ice momentum balance are defined, with particular attention payed to the internal ice stress in its various forms. A previously developed theoretical framework for modelling ice thickness, and hence deformation effects, is also included.

Five models are compared, four of which have their roots in the viscous-plastic model of Hibler (1979). The fifth (Gray and Morland, 1992) ascribes to no particular ice rheology. It is decided that the viscous-plastic model of Hibler and Walsh (1982) most suits the current needs of FOAM.

1. INTRODUCTION

The ocean circulation is driven primarily by the fluxes of heat, fresh water, and momentum across the air-sea interface, and these fluxes are in turn dependent on the current states of both ocean and atmosphere.

The Forecasting Ocean Atmosphere Model (FOAM) is planned to form the basis of an ocean forecasting system, making predictions of ocean temperature, salinity, and current structures up to a week ahead. FOAM will comprise of physically based numerical models of the atmosphere and ocean. The atmosphere model will be the same as that used for numerical weather prediction (NWP) by the Meteorological Office (Cullen, 1991) and the model of the ocean is derived from that of Bryan and Cox (1972).

Initially the weather forecast will proceed first, and predicted surface fluxes will be used to drive the ocean only run. Once the ocean data assimilation scheme has been proven then the sea surface temperature field from the initial analysis may be passed to the atmosphere model as the lower boundary condition for its calculations. Although the system could be run fully coupled, this is unlikely to be necessary.

The resolution of the NWP models will be determined by a number of factors. At the time of writing, the global model uses a 0.833° latitude by 1.25° longitude grid with 19 vertical levels. The present limited area model (LAM) also has 19 levels but has a horizontal resolution of 0.4425° for both latitude and longitude. The exact nature of the ocean model is as yet undecided, although it is likely to consist of a global grid with several higher resolution LAM's nested within. Initially the global grid size will be somewhere between a half and one degree, to be reduced to around a third of a degree whenever feasible. For the LAM's, a grid size of 10km is desirable.

In and around the polar regions, sea-ice can cover a large proportion of the sea surface. The production and subsequent motion of ice on the sea surface is of interest in its own right for its influence on shipping. In addition, the ice forms a buffer between the air and the sea, considerably reducing the transfer of heat and momentum between the two environments. Fresh water fluxes are also altered, with possible convective overturning of the upper ocean during ice formation, and stable stratification near the sea surface when it melts (§ 2A and § 2C). The refraction of sound waves within the ocean occurs because of vertical and horizontal gradients in the sound speed. The representation of ice-ocean interactions would give improved information on the temperature and salinity strucure of the ocean's interior and so (for example) aid the interpretation of SONAR signals, as would a knowledge of ice movement.

A globally applicable ice model has been sought for incorporation into the ocean component of FOAM. The model would need to usefully represent both the ice fields themselves and their influence on the surface transports (§3).

This document introduces the basic concepts used in sea-ice modelling and sets out the requirements for the FOAM ice model. Descriptions follow of the three main model options and, where possible, of their performance in simulations. Details of several derivatives of one of the of these (Hibler and Walsh, 1982) are included for completeness. The purpose is to clearly define the physical principles of each model so that a logical and justifiable decision can be made as to which one is most suitable for FOAM.

2 PHYSICAL PROCESSES

This chapter provides an introduction to the mechanisms involved in the formation, evolution, and motion of sea-ice, as well as some of its physical properties. The first three sections give a qualitative description of ice production and desalination, taken from Gow and Tucker (1990), whilst the rest of the chapter is concerned with the large scale representation and modelling of ice.

A. Cooling Of Sea-Water

Addition of salt to water depresses both the freezing point and the temperature of maximum density. When the salt content exceeds about 24.7 practical salinity units (psu), as it does in all the world's oceans, the water density increases monotonically as it cools, and this can produce instability and mixing (called convective overturning) in the ocean to a depth which depends on the temperature and salinity stratification. The whole mixed layer must then be cooled to its freezing point before ice formation can start.

B. Ice Formation

Initial ice formation occurs at or near the water surface as small platelets and needles called frazil. Under quiscent conditions the frazil crystals quickly freeze together to form a solid continuous ice cover between 1 and 10 cm thick. In rougher weather the combined action of wind and waves produces pancake ice - circular masses of semi-consolidated frazil ranging from 0.3 to 3.0 m in diameter. Eventually the pancakes consolidate fully by freezing together.

Once a continuous ice cover has formed, further crystal growth can only proceed smoothly if grain boundaries are perpendicular to the freezing interface and hence vertical column shaped crystals are produced. Each crystal comprises a number of parallel plates of pure ice. Salt cannot be incorporated into the pure ice lattice and much of it is expelled back into the ocean when ice forms. The rest resides in brine 'inclusions' between the pure ice plates. Typical overall salinities of newly formed sea ice are 5 to 15 psu depending on the rate of ice formation and the salinity of the freezing water.

C. Salinity Changes Within Ice

It has been found (e.g. Tucker et al., 1987) that the profile of salinity within sea-ice which has undergone at least one cycle of seasonal warming and cooling is substantially different from that of newly formed ice.

First year ice typically exhibits a C-shaped salinity profile, that is highest concentrations at the top and bottom of the ice. Summer melt drives a variety of processes (such as the production of drainage channels by expanding the brine pockets) which allow the bulk salinity of the ice to decrease and leave the upper ice virtually salt free.

Both ice formation and its desalination augment the salt concentration in the upper ocean. The resulting unstable density distribution can lead to convective overturning as described in § A. Conversely ice melt results in stable stratification - the ocean is topped by a light layer of fresh water. Systematic ice drift between specific source and sink regions can con-

tribute to the production of significant horizontal salinity gradients within the ocean.

D. Thermodynamics

Figure 1 depicts the vertical heat fluxes into and out of a layer of sea ice. It is conventional to represent heat flow into the ice as positive. Horizontal heat transports are omitted from the diagram for clarity

F_s and F_l are respectively the sensible and latent heat fluxes, and F_R and F_L are the incoming solar (shortwave) and atmospheric (longwave) radiations.

With surface albedo α, the reflected shortwave energy is αF_R.

If T_s is the temperature of the surface, ε_s its emissivity, and σ the Stefan Boltzman constant, the emitted longwave radiation F_T is $\varepsilon_s \sigma T_s^4$.

F_c is the conductive heat flux at the surface and can be expanded as $-k_I (\partial T/\partial z)_{z=0}$; similarly the conductive heat flux at the ice base F_b is given by $-k_I (\partial T/\partial z)_{z=-h}$; where k_I is the diffusivity of heat within the ice.

T_b is the temperature at the bottom of the ice, and T_w that of the mixed layer which is generally assumed to be isothermal. F_w is the heat flux from the deep ocean into the mixed layer.

In the models reviewed, the sea/ice interface is always assumed to be at the freezing point of the sea water so that a net positive bottom heat flux ($F_w - F_b$) causes melt and a net negative flux results in ice growth.

Shortwave radiation that passes through the ice surface (I_0) is absorbed by brine pockets in the ice interior (§ 2C). This allows internal energy storage and can cause the ice temperature profile to be altered and the brine volume to increase.

The system can be further complicated by snowfall which leads to an additional buffer layer between air and sea. Further, the presence of snow alters the albedo, the emissivity, and the temperature of the surface.

Regions of open water in an area with non-zero ice cover, termed leads, allow lateral melt and refreezing via horizontal heat transports. In some models it it assumed that there will always be some open water in each grid square due to natural wind variability and/or long term divergence and this takes the form of a minimum leads fraction. Further from each pole, the sea ice cover becomes both thinner and sparser. In the marginal ice zones, the interactions between individual floes are largely responsible for determining overall behaviour.

Ice and snow are generally split into one or more levels when modelled, and heat conservation and conduction laws are applied to each layer to give an overall thermodynamic growth rate f. For more detailed calculations, an ice thickness distribution function g(h) can be introduced such that g(h) dh is the areal proportion of the grid square that is covered by ice of thickness between h and h + dh. In general, g will be a linear combination of a smooth function representing the ice distribution, and a delta function $\delta(h)$ for the open water.

The governing equation for the thickness distribution function is

$$\partial g / \partial t = - \mathbf{div} (\mathbf{u}\, g) - d/dh (f\, g) + \psi + L_m \qquad [1]$$

Terms on the right hand side represent advection (with div as a two dimensional operator), thermodynamic growth, mechanical redistribution due to ridging and divergence (ψ; § 2G), and lateral melt (L_m; §'s 4D & 4F) respectively.

E. Ice Motion

Ice is generally treated as a plane lying on the ocean surface, and in this case the force balance can be written as

$$m\,(Du/Dt) = C + \tau_a + \tau_w + F + T \qquad [2]$$

where m is the ice mass per unit area, **u** the ice velocity and D/Dt the total rate of change (local and advective).

C is the Coriolis force, which in two dimensions can be approximated as

$$-m\ f\ \mathbf{k} \times \mathbf{u} \qquad [3]$$

where f is the coriolis parameter and **k** the unit vector upwards and perpendicular to the ice.

τ_a and τ_w are the air and water stresses respectively.

F is the ice interaction force which results from variations in internal ice stress (§2F).

T is the force which results from ocean surface tilt; it is associated with the geostrophic ocean currents and can be written as

$$-m\ g\ \mathbf{grad}\ H \qquad [4]$$

with g the acceleration due to gravity and H the dynamic height of the ocean.

The dominant components of this balance are the air and water stresses, the coriolis force, and the ice interaction term.

F. Internal Ice Stress

For modelling purposes ice is assumed planar and isotropic. Thus the internal ice stress ($\underline{\sigma}$) is a 2x2 matrix, where σ_{ij} is the force per unit length in the i direction acting on a line with normal in the j direction. Examination of the sum of the moments at the perimeter of an area element and the rate of change of its angular momentum (which should be the same as the sum of moments) shows that any anti-symmetry in the stress tensor will give rise to one term larger than all the others by a factor inversely proportional to the length scale of the element. As the infinitesimal limit is approached a clear inconsistency arises: hence the stress tensor is always symmetric. See Paterson (1983) for further details.

By a suitable transformation of the co-ordinate axes, the shear components of the stress tensor can be made to disappear while the normal components reach extreme values. These maximal components are termed principal stresses, and the transformed axes are known as the principal axes. Both depend only on the state of the stress at the point in question, and are thus independent of the reference frame. The principal stresses are the eigenvalues of the stress tensor,

$$(\sigma_{11} + \sigma_{22})/2 \pm [1/4\,(\sigma_{11} - \sigma_{22})^2 + \sigma_{12}\,\sigma_{21}]^{1/2} \qquad [5]$$

and the principal axes are the corresponding eigenvectors. It is well known that the eigenvectors of a symmetric matrix are orthogonal provided their corresponding eigenvalues are

unequal (e.g. Anton (1984)); hence the principal axes are purely a rotation of the reference axes.

Bulk stress (σ') is the combination of stress components which tends to change the volume of an element. It is the sum of the eigenvalues,

$$\sigma' = (\sigma_{11} + \sigma_{22}) \qquad [6]$$

Shear (or deviatoric) stress (σ'') tends to change the shape of an element, and for a 2x2 tensor it is the difference between the eigenvalues,

$$\sigma'' = \det(\underline{\sigma} - \sigma' \underline{I}) = ((\sigma_{22} - \sigma_{11})^2 + 4\,\sigma_{12}\,\sigma_{21})^{1/2} \qquad [7]$$

where $\underline{I}$ is the identity matrix.

These are both combinations of the principal stresses and are known as the stress invariants.

Figure 2 shows the above three ways of representing a given stress state in a two dimensional system.

Strain is denoted by the tensor $\underline{\varepsilon}$. If the strain were applied to a unit vector in the i direction, then ε_{ij} is the amount the vector would stretch in the j direction. The rate of strain tensor e_{ij} represents the change in the i component of particle speed that would accompany a unit displacement in the j direction. Note that, unlike the stress tensor, strain and strain rate may have anti-symmetric components. For the purposes of ice modelling, however, symmetry is assumed.

Concepts analogous to the principal stresses and the stress invariants exist for strain and strain rate.

It is useful to express the strain rate invariants in polar co-ordinates,

$$|e| = (e'^2 + e''^2)^{1/2} \quad \text{and} \quad \theta = \tan^{-1}(e'' / e') \qquad [8]$$

N.B. In pure divergence or pure convergence: $|e| = \mathbf{div}\ \mathbf{u}$ = bulk strain rate.

In some early models, ad hoc corrections to ice velocity were made to approximate its fluid properties. Nowadays, most models relate $\underline{\sigma}$ to $\underline{\varepsilon}$ and/or $\underline{e}$ via a constitutive law and the internal ice stress $\mathbf{F}$ is calculated by

$$F_i = \partial\sigma_{ij} / \partial x_j \qquad [9]$$

The constitutive equation contains coefficients related to the bulk and shear viscosities of the ice, and in many cases an ice strength (§ 2G). It attempts to describe the mechanical properties of the solid/fluid in question. Three idealised rheologies are usually used, either singly or in combination:-

In an **elastic** material, stress depends purely on the strain state. A special case, linear elasticity in one dimension, has stress as a constant multiple of strain - Hooke's Law.

In a **viscous** substance, stress depends purely on strain rate. The familiar Newtonian viscous fluid is linearly viscous.

Ideal plasticity, or **rigid plastic** behaviour means that (in one dimension for simplicity) there is no strain in the material until a specific yield stress is reached. The yield stress is the maximum internal resistance that the material can put up in order to oppose deformation; and if external forces exceed it then the material strains indefinitely at indeterminate speed. In two dimensions the regions of strain and no strain are separated by a yield curve, drawn

with the principal stresses or the stress invariants as co-ordinate axes.

G. Ridging, Rafting, and Divergence.

Mechanical redistribution of the ice will occur when the combined stresses within the ice lie outside the bounds of the yield curve (if a plastic model is being used); if a viscous model is applicable then any non-zero stress divergence (see equation [9]) will generally result in redistribution; in the case of an elastic material, a change in the stress divergence is needed.

In the case of divergent motion, the ice generally cracks to form open water. Convergent motion produces rafting - thin ice floes sliding on top of one-another - or ridging, wherein ice blocks (called rubble), formed by the buckling and bending of an ice sheet, are piled both above and below the surface. The above surface portion of such a pressure ridge is called the sail, that below the surface is the keel. The much increased roughness length of a ridged sea/ice interface is responsible for increased mixing of the upper ocean, known as keel stirring.

The effects of convergence are often grossly simplified in numerical models (for example by a universal increase in ice thickness through a grid square), but the introduction of a mechanical redistribution function ψ (h,g) based on a specific ice deformation model allows a more general (though complex) approach. The redistribution function describes the time rate of change of g(h) - the thickness distribution - due to mechanical deformation.

Thorndike et al. (1975) describe a theoretical framework designed to allow calculation of ψ and hence deformation effects:-

1.Thinner ice is more likely to deform than thicker ice and so a breakability weighting b(h) is required, such that a(h) = b(h) g(h) is the distribution of ice about to be ridged. Thorndike et al. (1975) suggest a weighting that only allows the thinnest 15% of the ice (including leads) to ridge. Within this band, thinner ice is still more likely to deform.

2.A mathematical representation of the ridging process, $\gamma(h_1,h_2)$, is also required such that $\gamma(h_1,h_2)\, dh_2$ is the area of ice put into the thickness interval $[h_2,h_2+dh_2]$ when a unit area of ice of thickness h_1 is used up by ridging. For example, Thorndike et al. (1975) adopt the simple hypothesis that ridging multiplies the ice thickness by a factor k, that is $\gamma(h_1,h_2) = \delta(h_2-kh_1)$.

3.The ridging rule and the distribution of ice to be ridged combine to give z(h), the distribution of ice after ridging. The amount of ice put into the thickness interval [h,h+dh] when a unit area of ice is ridged is z(h) dh. Note that the total area under the redistribution curve is generally less than one as the grid area covered by a particular section of ice decreases on ridging.

4.Knowledge of the pre- and post- ridging distributions allows calculation of the ridging mode $w_r(h,g)$, the change in g per unit strain under pure convergence (i.e. 1/dA times the change in g that would occur if a unit area of ice were compressed to area 1 - dA).

5.Treating leads as ice of zero thickness, and assuming ice has zero tensile strength, the ridging mode under pure divergence is a delta function $\delta(h)$. A strain dS on a unit area produces area dA (a number equal to dS) of open water.

6.A given large-scale strain rate can involve both lead and ridge formation on the smaller scale, and the strain weighting functions $\alpha_0(\theta)$ and $\alpha_r(\theta)$ give the relative production

rates per unit strain compared to pure divergence and convergence. They can be assigned any form subject to the conditions imposed at $\theta=0$ and $\theta=\pi$ by their definitions.

The mechanical redistribution function is then given by

$$\psi = |e| [\alpha_0(\theta)\, \delta(h) + \alpha_r(\theta)\, w_r(h,g)] \qquad [10]$$

Ice can withstand much greater stress under compression than under tension and this is often reproduced by way of an ice strength P, the maximum compressive stress that the ice rubble can take before yielding, the resistance it applies when yielding, and equivalently the work done per unit area per unit strain under pure compression. A form for P (dependent on ice thickness and concentration) is either decided arbitrarily, or P is split into a frictional component P_f and a potential energy component P_p as suggested by Rothcock (1975). The rate of loss of energy by friction per unit area ridged is then $|e|\, \alpha_r(\theta)\, P_f$. The same quantity is estimated by an alternative method and equation of the two sets a value on P_f. Bratchie (1984) assumes ice sheets and rubble of the same thickness slide as one item into the side of a ridge, penetrating between the sail and the keel, whilst Hibler (1980) takes frictional losses to be of the same order as potential energy creation (i.e. P_f is set equal to P_p).

The time rate of increase in potential energy during ridging is

$$C_b \int_0^\infty h^2 \psi \, dh \qquad [11]$$

where C_b is a combination of gravitational acceleration and ice and water densities which accounts for both sail and keel formation in isostatic equilibrium. Now P_p is the increase in potential energy per unit area per unit strain, hence

$$P_p = C_b \int_0^\infty h^2 w_r(h,g)\, dh \qquad [12]$$

3. OUTPUTS

The FOAM ice system will supply information to the Royal Navy as well as feeding data directly into the atmosphere and ocean models. The nature and required quality of these three overlapping outputs is now considered.

A. The Navy need direct outputs of mean ice thickness and concentration within each grid square, and an indication of ice edge position. Additional information such as ice type, floe size and ice thickness distributions within each square, and the rates of ice drift, convergence, and divergence would be useful but not essential and the model could be modified for their inclusion at a later date.

B. The ocean model requires heat, momentum, and salinity fluxes as inputs from both the atmosphere model and the ice model. In the atmosphere model, the salinity flux will represent the combined net precipitation and evaporation at the ocean surface, and in the ice model it will relate to the rates of ice formation and melt.

C. At first, the atmosphere model will require only ice concentration and depth in each grid square, from which it will make its own estimates of ice and sea surface temperatures. As closer coupling becomes feasible, the transfer of assimilated ice and sea surface temperatures, and then predicted surface temperatures as well as parameters such as snowcover, meltponds, and related albedo variations might be possible.

For the future, it is also conceivable that one or more higher resolution regional ice models may be required, possibly entailing the inclusion of more detailed and/or area specific physics.

4. ICE MODELS

This chapter provides a review of three complete ice models which are candidates for use in FOAM. Brief descriptions of several other models are included, either because they form the basis of parts of more recent models, or they highlight different approaches

The ice models to be considered have generally been applied to the Arctic. It is worth pointing out a few general features of this region for comparison with the model results (fig. 3 shows the geography of the Arctic).

Two main systems characterise the surface currents of the Arctic; the Transpolar drift, in which the surface waters and ice of the Eurasian Basin move across it towards the North Pole and then on towards the Fram Strait (between Greenland and Spitsbergen). There is also the anticyclonic (clockwise) Beaufort Gyre in the Canadian Basin.

Much of the heat and water exchange between the Arctic and the rest of the world's oceans occurs in the Fram Strait. The West Spitsbergen Current, an extension of the Norwegian-Atlantic Current, carries warm, relatively salty water northward into the Arctic. The East Greenland Current defines the main flow out of the Arctic.

The average extent of sea ice in the Arctic typically varies from $7x10^6$ km^2 in the summer to $14x10^6$ km^2 in the winter. Mean thicknesses for unridged multiyear ice are about 3m, and even near the pole the ice thickness is usually less than 4m . However deformation tends to build up the ice off the north coast of Greenland and the Canadian Archipelago, with thicknesses of over 6m measured there.

A. Thermodynamic Only Models

Maykut and Untersteiner (1971) detail a very high resolution (up to 40 layers, each 10cm thick) one dimensional thermodynamic model which predicts the time evolution of an ice slab subject to climatological atmospheric energy fluxes, constant ocean heat flux, and proscribed snowfall. The model solves the heat diffusion equation, with a Beer's Law term for penetrating short wave radiation, inside the ice and snow. The thermal diffusion coefficient and specific heat vary with temperature and salinity according to the approximate formulae of Untersteiner (1961), salinity being estimated from an assumed profile shape, similar to that of multiyear ice. Penetrating solar radiation, absorbed by brine pockets becomes part of the temperature - salinity - brine volume calculations. Albedo is allowed to vary with ice thickness.

Semtner (1976) simplified the Maykut and Untersteiner model, reducing the number of internal temperature points to a maximum of two in the ice and one in the snow (called the three layer model), and changing the numerical algorithm for solving the heat diffusion equations. Penetrative radiation was accumulated in an internal heat storage reservoir and used to keep the temperature near the surface of the ice from dropping below the freezing point in the early part of the cooling season. Ice and snow densities, specific heats, and diffusion coefficients were fixed. A simplified "zero layer" model which calculated no internal temperature points, merely balancing the surface and bottom fluxes, was also considered. It only used three prognostic variables (ice thickness, snow thickness, and surface temperature) and assumed a linear temperature profile throughout the snow/ice or ice layer.

The model of Maykut and Untersteiner (1971) is a carefully formulated, comprehensive

treatment of sea ice thermodynamics and was used as a standard against which to test the more simplified models of Semtner (1976). Thickness predictions were compared over a whole range of scenarios and a very high correlation was achieved with the three layer model throughout each seasonal cycle. The one layer model performed just as well on annual means but the amplitude and phase of the seasonal variation were somewhat distorted, as is only to be expected with an algorithm equivalent to instantaneous adjustment throughout the ice and snow to external temperature changes.

Washington et al. (1976) extended the simple Semtner model to the horizontal and included a leads variable at each grid point to represent the fraction of open water present. This allowed lateral melting and freezing, the latter resulting in a new mean thickness and an increase in the ice concentration to its maximum value. The study showed that the introduction of leads allowed simulation of a reasonable seasonal cycle but regional variations in ice thickness and total amount of ice production were unrealistic; for instance, maximum ice depth occurred in the central Arctic.

B. Dynamic Thermodynamic Models

Parkinson and Washington (1979) built upon the model of Washington et al. (1976), using a more sophisticated leads parameterization in which (for a positive lead heat balance) the larger the lead area, the more energy was used to directly warm the lead rather than melting the ice laterally. For a negative heat balance the ice fraction was increased but ice thickness remained unchanged. The ice interaction term in the momentum equation [2] was ignored, to give the free drift velocity, which was then corrected iteratively under convergence to maintain a fixed minimum fraction of leads.

The results were not too different from those of Washington et al. (1976) with maximum thickness still occurring at the centre of the Arctic basin. The velocity correction appeared to be stopping all motion rather than realistically modifying the relative velocities.

Addition of a constitutive law (3F) into the model physics allows a complete momentum balance. The Arctic Ice Dynamics Joint Experiment (AIDJEX) which took place between 1970 and 1977 provided measurements of the different terms entering the momentum equation and lead to the development of the AIDJEX model (Coon, 1980). This contained an elastic-plastic constitutive law, allowing ice to resist compression as an elastic material until stress caused ridging, from which point the ice compresses plastically. This had the advantage that the ice could remain stationary under a variety of small stresses but the inclusion of elasticity necessitated keeping track of the strain state for a given portion of the ice indefinitely. It forced a Lagrangian formulation and introduced substantial mathematical complexities.

To avoid this whilst still retaining plastic behaviour, Hibler (1979) considered ice to be a non-linear viscous plastic compressible fluid. With such a rheology the ice would deform plastically for high strain rates, presenting a resistance to the deformation determined by the yield curve. When experiencing low rates of strain, ice resistance would be viscous. Thermodynamic growth rates were proscribed as functions of ice thickness and the time of year; they were estimated from experimental data.

Hibler (1980) upgraded his previous work to include thermodynamics similar to those of Semtner (1976), a thickness distribution, and a ridging rule to account for mechanical deformation and derive an ice strength. The US Polar Ice Prediction System (PIPS) (Riedlinger and Preller, 1991) is based upon the model of Hibler and Walsh (1982) which dropped the

explicit ridging rule and ice thickness distribution but kept the thermodynamics. This is one of the options for FOAM.

C. The Viscous-Plastic Model of Hibler and Walsh (1982)

C1. The Model

A linear temperature profile is assumed throughout the ice and the effects of snow cover are parameterised only by changing the surface albedo of the ice to 'snow' values for surface temperatures below freezing.

The basic surface heat balance equation in the presence of an ice cover is then

$$(1-\alpha)F_R + F_L + D_1 u_G (T_a - T_s) + D_2 u_G [q_a(T_a) - q_s(T_s)] - \sigma\varepsilon_s T_s^4 + (k_I/h)(T_b - T_s) = 0 \qquad [13]$$

with α, F_R, F_L, T_s, T_b, and k_I as defined in §2D, D_1 and D_2 bulk sensible and latent heat coefficients, u_G the geostrophic wind speed, T_a the air temperature (at 10m), and q_a and q_s the specific humidities of the air at 10m and just above the ice surface.

It can be seen that standard bulk equations for latent and sensible heat are used and penetrating radiation and internal heat storage are ignored.

The balance can can be rewritten as

$$A_1 + A_2(T_s) + (k_I/h)(T_b - T_s) = 0 \qquad [14]$$

with A_1 independent of T_s, and A_2 a non-linear function. This equation is solved for T_s using a Newton-Raphson procedure, with T_s then set to the freezing point of fresh water (273.16K) if the calculated value exceeds it. If this occurs then the excess energy that would have increased the ice temperature to T_s is used to melt the ice. The mixed layer is fixed at 30m deep (although this is not intrinsic to the ice model itself - in FOAM the mixed layer will be a part of the ocean model and variable in depth) and its temperature is constrained to the freezing point of water if there is any ice in the grid square. The growth rate of ice is then

$$f_B(h) = -[A_1 + A_2(T_s) + F_w] / Q_I \qquad [15]$$

with Q_I the volumetric heat of fusion of ice.

The full momentum balance equation [2] is used. Air and wind stresses are estimated from the quadratic formulae

$$\tau_a = \rho_a c_a u_G [u_G \cos\theta + k \times u_G \sin\theta] \qquad [16]$$

and

$$\tau_w = \rho_w c_w |u_w - u| [(u_w - u)\cos\phi + k \times (u_w - u)\sin\phi] \qquad [17]$$

where ρ_a, ρ_w, c_a, c_w, θ, and ϕ are the air and water densities, drag coefficients, and turning angles (assumed constant) respectively. The geostrophic ocean currents u_w are computed from long term mean values of sea surface height (FOAM will use input from the ocean model).

Internal ice stress is modelled with the constitutive law

$$\sigma_{ij} = 2\eta e_{ij} + [\zeta - \eta] e_{kk} \delta_{ij} - P \delta_{ij}/2 \qquad [18]$$

where ζ and η (kg s^{-1}) are related to the bulk and shear viscosities of the ice, and P is

the depth integrated ice strength (Nm^{-1}). Except for the pressure term, this is the same form as for a general isotropic fluid with linear stress-strain relation (i.e. $\sigma_{ij} = \Lambda_{ijkl}\, e_{kl}$ with Λ isotropic) and is considered appropriate for ice. However the viscosities are made dependent on pressure and strain rate so that for most strains the stress state lies on the solid elliptical yield curve shown in figure 4. Roughly, the viscosities are proportional to the inverse of the strain rate so that for very small rates of strain they can be extremely large. To avoid this, high limits on the viscosities are chosen and on the rare occasions when they are reached, the stress state lies inside the yield ellipse; the dotted curve in figure 4 provides an example of this viscous part of the rheology.

The ice distribution is split into 'thin ice' which represents the combined fraction of open water and ice up to some cut off thickness h_0 (Hibler takes h_0=0.5m) and 'thick ice' which accounts for the remainder of the grid square. To keep track of the ice cover, two variables are calculated, the mass of ice in the cell (in the form of an equivalent ice thickness h) and the compactness A - the fraction of thick ice in the cell.

Continuity equations for mean thickness and compactness

$$\partial h/dt = - \partial(uh)/dx - \partial(vh)/dy + S_h + \text{diffusion} \qquad [19]$$

$$\partial A/dt = - \partial(uA)/dx - \partial(vA)/dy + S_A + \text{diffusion} \qquad [20]$$

account for advection of cell properties and thermodynamic growth (S_h and S_A) as obtained from the heat balance calculations. The diffusion terms are added to keep fields smooth during long integrations.

Compactness is confined to the interval [0,1] and therefore, when the upper limit is reached, a sink term is brought in to the equation which converts further convergence to a uniform increase in 'thick ice' thickness.

Thermodynamic ice depth change rate (S_h) is the weighted mean of calculated growth rates over both 'thick' and 'thin' ice. Freezing in leads increases compactness by the amount of ice of thickness h_0 that could be created given the heat budget over open water. Compactness decreases due to melt are obtained by allocating to the 'thick' ice a uniform thickness distribution between zero and twice its mean thickness and a growth rate of S_h.

Compressive ice strength P is coupled to thickness and compactness via the expression

$$P = P^* h \exp[-c(1-A)] \qquad [21]$$

where c and P* are fixed empirical constants. This formulation, itself empirical, makes the strength strongly dependent on the amount of thin ice, while also allowing the ice to strengthen as it becomes thicker.

C2. Results

Using observed 8 day mean geostrophic winds from a one year period as forcing, Hibler (1979) obtained realistic mean arctic ice thickness, compactness and velocity distributions. The Beaufort Gyre and Transpolar Drift stream were reproduced (fig. 5), as was the ice build up off the Canadian Archipelago. Ice thicknesses off northern Greenland were overestimated and those off the Siberian Coast underestimated, but the general contour shape and positioning agreed qualitatively with submarine sonar estimates. Autumn and winter compactness values of greater than 95% were simulated over most of the Arctic, in general agreement with submarine observations. The summer compactness values were similar to the observed values for relatively ice free summers - such as that which occurred in the year

from which the forcing data was taken. Ice extent could not be examined because the model grid covered too small an area.

Hibler and Walsh (1982) used the dynamic thermodynamic ice model in the first attempt at simulating the sensitivity of seasonal features to interannual fluctuations in the forcing fields. Observed daily atmospheric forcing was from the three year period 1973-75 and the model grid was enlarged to cover not only the Arctic Basin but also the peripheral seas and the marginal ice zone. Figure 6a shows simulated ice edge positions and mean simulated ice thickness, the latter in good agreement with observed values. Comparison with observed ice extents (fig. 6b) however shows serious discrepancies, the most prominent being the excessive ice production in the north Atlantic in winter and spring. This was attributed to the absence of horizontal ocean heat transports in the model but may also be associated with a lack of deep convective mixing due to the use of a fixed depth mixed layer. Summer melt was also exaggerated in the simulation.

Interannual variations were calculated by examining the total area within the ice edge and the total ice covered area. Three year mean values for each month were subtracted from the monthly means for each year individually. Both observed and simulated plots showed similar amplitudes and they were all positively correlated, with the best correspondence in the Alaskan and Siberian sectors and the worst in the North Atlantic.

Walsh et al. (1985) ran an expanded model, with prescribed snow and ice thickness distributions about the mean, and using continuous forcing fields from 1951 through to 1980. The additional thickness levels allowed even more summer melt and winter freezing, giving again a too large seasonal amplitude. Closer examination of the energy budget revealed that most of the summer melt occurred at the top surface and was at least partially due to the omission of short-wave penetration and internal energy storage in the model physics. The model did not include a stably stratified summer ocean which would limit heat transport from the deep ocean and it is possible that the single slab thermodynamic treatment systematically underestimated the sea ice growth rate. The simulated wintertime north Atlantic ice edge was 5-10 degrees south of its mean observed position and this was again attributed to lack of oceanic effects - more specifically the convective overturning caused by the cooling of surface waters which carries warm water upwards.

Interannual variations all correlated positively with observations. Values ranging from 0.4 to 0.9 were obtained for different longitudinal sectors. The lightest and heaviest summers (with respect to Alaska and Siberia) are shown in figs. 7a and 7b. The overall bias to excessive summer melt is readily apparent but the differences in ice extent between the two pictures is fairly well simulated, except in the north Atlantic. Simulated buoy drift rates showed negligible bias but considerable scatter about observations.

Hibler and Bryan (1987) combined the Hibler and Walsh (1982) model with the multi level baroclinic ocean model of Bryan (1969). The whole ocean, bar the uppermost (mixed) layer was, relaxed towards climatological temperature and salinity data to give a 3 year equilibrium time scale. The idea was to allow daily and seasonal mixed and upper layer variability whilst prescribing and fixing the deeper oceans. The observed daily geostrophic winds from 1979 and climatological surface air temperatures and mixing ratios were used to force the model. For comparison, a parallel run was performed, replacing the ocean model with a stationary, fixed depth mixed layer.

The models produced a weak ice build up against the Canadian Archipelago and an unrealistically large build up against the Siberian coast. This was due to the somewhat atypical ice model transport caused by the unusual winds of 1979. Overall, inclusion of the full ocean

model consistently improved the predicted ice drift magnitude and turning angle and it especially improved the simulated drifts in the East Greenland Sea (N. Atlantic) over the ice only run. The full ocean ice model could support convection and overturning and showed a much improved accuracy in predicted ice advance and persistence from December to April in the North Atlantic (fig. 8). The oceanic treatment was less effective on the retreat phase, which continued to simulate excessive decay over the summer.

D. The Full (Uncoupled) Viscous-Plastic Model

As mentioned earlier, Hibler (1980) introduced an ice thickness distribution g(h) to the model satisfying the governing equation [1].

The lateral melt term was calculated from two coupled equations; the first forced the mixed layer temperature to decrease in proportion to the mass of ice removed by lateral melting and increase in proportion to the heat absorbed by the lead that was not used to increase the rate of vertical melt. The second equation ensured that enough instantaneous lateral melt would occur to either lower the mixed layer temperature to freezing or remove all the ice. from the grid square.

Redistribution was taken to be constant up to a cut off ridge height (the distance from the tip of the sail to the top of the keel) h_2 and zero thereafter, which corresponded to a triangular ridge profile of maximum height h_2. A geometrical argument justified the chosen dependence $h_2 = 2\,(H^* h_1)^{1/2}$ with H^* an empirical constant. The minimum thickness of any ridged ice was taken to be twice the original ice thickness (h_1). The mechanical redistribution function was calculated as detailed in § 2G, with the same breakability weighting as suggested by Thorndike et al. (1975).

E. The Cavitating Fluid Model

Flato and Hibler (1990) produced a simplification of the Hibler and Walsh (1982) model which ignored any shear and tensile strength of the ice, yet retained a compressive ice strength.

New, linear ocean and air (for consistency) stress equations were used as a linear momentum equation was needed for the numerical system to work:

$$\tau_a = \rho_a c_a \, [u_G \cos\theta + k \times u_G \sin\theta] \qquad [22]$$

and

$$\tau_w = \rho_w c_w \, [(u_w - u)\cos\phi + k \times (u_w - u)\sin\phi] \qquad [23]$$

with variables as defined in section 2C. To aid comparison, new drag coefficients were chosen to give the same mean annual stresses (from the same input fields) as in the run of Hibler (1979).

Each square grid cell contained an ice pressure at its centre and ice velocities at each of its four corners. In the equation of motion, the total time derivative was ignored as it is relatively small, and internal ice pressure was initially set to zero to allow the straight forward calculation of free drift ice velocities.

After the free drift velocities had been found, an iterative procedure corrected the ice pressure and velocities in each cell to allow for the compressive strength of the ice. The pressure increment dP that would be needed to negate all convergence was calculated for each grid square in turn. If the sum of the current pressure in the grid square (P) and the incre-

ment (dP) was less than the compressive strength P_{max} of the ice then the increment was applied to the grid square; otherwise the increment was limited to $(P_{max}-P)$. The increased horizontal pressure gradient was then allowed to perturb the ice velocity component that was parallel to it - thus the Coriolis force and off diagonal wind and water stress terms were ignored when correcting the free drift velocity.

This whole process swept the grid a number of times - until the velocity changes from one iteration to the next were negligible.

For daily forcing, the cavitating fluid model was twice as fast as the standard viscous-plastic model, but there was little difference in cost if monthly mean forcing was used. With daily forcing, estimated velocity magnitudes from the cavitating fluid model were very similar to those of the standard viscous plastic model, but the calculated monthly outflows from the Arctic were approximately doubled in late spring/early summer and halved throughout the rest of the year. Ice thickness fields were of similar shape but there were differences in magnitude and in the representation of smaller scale features.

F. The Bratchie Model

Bratchie (1984) produced a major modification of the Hibler (1980) model, suitable for smaller scale applications in and around the marginal ice zones. Theoretical developments in the thesis allowed calculation of two further output fields - ice floe size and number - for each grid square. Further, from a theoretical ridging model and a few other basic assumptions, an ice strength and an explicit formula for a yield curve were obtained. The model was tested in the East Greenland Sea.

Ice floe fields were modelled with three parameters: compactness A (as with Hibler's models), the mean number of floes (assumed squat and cylindrical for simplicity) per unit area, n , and mean floe radius r , such that $A = n \pi r^2$.

Firstly, the ratio L, the number density of floes near a particular reference floe compared to the overall number density (n), was estimated as a function of compactness (note $L>1$ as the reference floe is guaranteed to lie in the area considered). The one dimensional version of this problem has an analytical solution and a solution of analogous form was postulated for the two dimensional situation. The arbitrary constants were set by applying known high density (close packed) and low density limits, to give a simple equation for L.

Collisions were examined with respect to large scale differences in mean drift velocities rather than small scale bumping, about which no information was available. The first (non-zero) term in the two-dimensional power series expansion was used to approximate the velocity field relative to the reference floe,

$$\mathbf{u(x) = x \,.\, (grad\ u)}_{\mathbf{x=0}} \qquad [24]$$

The velocity gradient was related to the strain rate at the origin giving a collision rate per unit area of

$$2\, n\, L\, A\, |el\, \alpha(\theta) \qquad [25]$$

The collision rate relative to that which would occur in pure convergence, $\alpha(\theta)$, was derived analytically.

Floes involved in collisions were assumed to stick together and ridge (see later). Experimental evidence points to tilting and bending of the ice floe as the major mechanism for floe break up, and flexible beam theory was utilised to describe this.

For calculating thermodynamic changes a floe number density distribution n(h) was introduced, such that $\int n(h)\, dh = n$. The number density satisfied an equation analogous to that for the thickness distribution [1].

Bratchie (1984) examined analytically a shallow rectangular ice block, with the ice touching the sea just warm enough to melt and the ice touching the air at a constant low temperature. He found that the lateral melt rate is $\pi/2 + 2/\pi$ (≈ 2.05) times the vertical melt rate and incorporated this into the heat budget equation.

The model used the full momentum equation [2] with air and wind stress formulations identical to those of Hibler (1979). An ice thickness distribution function g(h) was used as by Hibler (1980).

Ridges were all assumed to be of similar shape (fig.9) defined by θ^a and θ^b, the respective angles of the sail and keel to the horizontal. Ridge size was defined by the unridged ice thickness, h_1 , and the distance from the tip of the sail to the bottom of the keel, h_2. Isostasy gave the position of sea level relative to the ridge.

First the final size of a ridge, characterised by its height (h_2) , was estimated. The ridging strength of the ice was defined to be the maximum stress an ice sheet can withstand before it shatters into rubble and deforms plastically into ridges. It was taken as

$$P = 9000\, h_1 \ Nm^{-1} \qquad [26]$$

Note that the compressive strength of the ice rubble is the resistance it puts up to pure compressive, plastic deformation, as defined in §2G. Both the compressive and ridging strengths used by Bratchie were effectively depth integrated yield stresses.

Bratchie estimated maximum ridge height from the following approximation to the ridge building process:

When two ice sheets meet and the internal stresses generated exceed the ridging strength then a certain amount of rubble is generated. The whole ridging process is assumed instantaneous and so the ice sheets continue to converge, piling up the rubble into a triangular prism as defined by θ^a , θ^b , and volume conservation. Moreover, if the ice sheets meet, the ridging strength will still be exceeded and more rubble will be generated. This process will continue until the maximum work that can be done by each of the ice sheets moving a distance dl towards the ridge centre is just less than the sum of the work that would need to be done against friction by the ice sheets and rubble and the potential energy that would be needed to displace thickness 2 dl of rubble from the ridge centre to create a new, slightly larger triangular ridge.

By definition, P dl is the maximum work that each ice sheet can do. The potential energy required to increase the ridge height was easily derived, and the frictional energy loss was calculated from the simple sliding model described (briefly) in §2G. Equating the total energy needed to cause an increase in ridge height with the maximum energy obtainable from the converging ice sheets gave the ridge height $h_2(h_1)$.

The known ridge profile implied a specific ridging law which was then substituted into the algorithm of Thorndike et al. (1975) to give the compressive strength of the rubble. Bratchie (1984) used the same breakability weighting as Hibler (1980) and Thorndike et al. (1975) and made the simplest possible assumption about the strain weighting under ridging $\alpha_r(\theta)$: that it was the same as the strain weighting under floe collision $\alpha(\theta)$. This assumption is sensible for low floe densities and it turns out to be acceptable for continuous ice cover. It may not be valid for the intermediate situations such as when the ice cover consists of

highly compacted floes.

Using the same basic constitutive law as Hibler (1979) [18], Bratchie (1984) then derived the yield curve shown in figure 10.

Initial conditions for the model run were taken from data for 30/11/78. Forcing consisted of twice daily wind fields and atmospheric temperature data from ECMWF. Long term geostrophic currents were reduced by a constant factor before inclusion to attempt to parameterise the meandering of the currents. The grid length was 35km - about one sixth of that used by Hibler and Walsh (1982) - and allowed fairly detailed model descriptions.

After just one month, the observed and simulated ice edge positions had already started to diverge; a large number of small (1-10m), thin (<1m) floes were predicted several hundred kilometres past the observed 3/8 compactness line. Wave action was the suggested culprit; it would have broken up thin ice near open water whilst leaving unaffected the thick floes away from the ice edge. However the inclusion of wave effects would have necessitated substantial reworking of the model.

The best agreement between model and reality occurred in the second half of May 1979, by which time most of the thin ice had melted. Bratchie pointed out that if ice less than about 30cm thick is ignored, then the model predicts more or less correct values for total ice extent during most of the run.

Comparison with a satellite photograph for 9^{th} May 1979 revealed good relative positioning of the main pack of large floes. Another area of loose pack is also correctly positioned by the model but its size is overestimated. Although they may have been present in reality, other predicted features are not visible in the satellite picture.

G. The Model Of Gray And Morland

Gray and Morland (1992) derived a full set of 3-dimensional equations for thermodynamic and dynamic processes in and around a single ice floe on a flat earth. The description was kept as general as possible, with only a few basic assumptions made, such as ice density and specific heat being temperature independent and the vertical Coriolis force being negligible. Depth integrated equations were obtained and these were simplified using two small parameters:

$$e^* = h^*/l^* = 5\times10^{-6} \qquad [27]$$

$$\text{and} \quad e_f = h^*/l_f = 5\times10^{-3} \qquad [28]$$

where $h^* = 5m$ is the depth scale of an ice floe, and $l^* = 10^6$ and $l_f = 10^3$ are the horizontal length scales of polar weather systems and ice packs and of individual floes respectively. Vertical velocity components and non-rigid velocity changes across a floe span were shown to be negligible.

The basic assumption was that changes in all variables across a floe span are smooth and (at their largest) no greater than changes through thickness h^*, but changes across the pack or weather system scale are comparable in size with changes through the ice thickness.

Individual floes were ignored on the pack scale, the system being treated as a 2-dimensional ice/water mixture with ice and water velocities and partial densities defined everywhere. This assumption is a compromise as the next stage would be to track individual floes, which is beyond the capabilities of current models.

A contact length function (f) of local compactness was introduced, such that f(A) was the proportion of a floe edge that was in contact with other ice floes. The total extra stress was defined as the stress over and above that due to water pressure, and the extra traction as the corresponding force on a particular plane. Edge tractions due to water were assumed to be dominated by the pressure term and so did not contribute to the extra stress or extra traction terms. For simplicity, a uniform, homogeneous floe distribution and shape was taken. Several similar constitutive laws were postulated which corresponded to no specific rheology and gave the extra edge tractions between two touching floes in terms of the local strain rate. The calculated edge tractions were integrated around the floe edge and through the floe depth and the result was multiplied by the contact length factor and the local compactness and divided by the floe area to give the local area mean of depth integrated extra stress. Equation [9] then gave the internal ice force for input into the momentum equation.

Governing equations for A and h under divergence were the same as those of Hibler (1979 etc.) except that the scheme of Gray and Morland needed no diffusion. Under convergence Hibler's simple scheme was not applied, instead compactness was split into coherent ice fraction A_c not in failure, which moved horizontally, and ice fraction A_r available for ridging. The latter was (naturally) zero in diverging floes, and in converging floes it increased monotonically from 0 to 1 as compactness increased:

$$A_r = r\,A \quad \text{and} \quad A_c = A\,(1 - r) \qquad [29]$$

with r a function of compactness, $d/dA\,(rA) \geq 0$ and $r(1) = 1$. A further condition on r was necessary to ensure that the speed of ridging was enough to stop the compactness exceeding unity. Ridging ice was assumed to redistribute uniformly and instantly, the rate of increase of height being determined by the strain rate, volume conservation, and a prescribed rate of transfer between coherent and ridging ice. The heights of both ridging and coherent ice were tracked separately during convergence, but were merged to an area weighted average when convergence (and hence ridging) ceased.

A standard thermodynamic treatment, with penetrating radiation but no brine pockets or snow cover, was used.

The model is still being developed, functions for the coherent ice contact proportion (f) and te ridging fraction (r) have been suggested but no complete model runs have yet been performed.

Gray and Morland point out that Hibler gives no precise definition of his stress term $\underline{\sigma}$. Consistency of the momentum equation of Hibler with the balance of Gray and Morland forces $\underline{\sigma}$ to be the two dimensional depth integrated extra stress as expected. It is also shown that implicit in the momentum equation of Hibler (1979) is the assumption that the layer of water and thin ice moves freely in the leads, unimpeded by the surrounding thick ice. With this in mind, it is apparent that Hibler was purely examining the motion of the thick ice layer and ignoring all motion within the leads, assuming that it did not interact with the thick ice. In this case only the wind and water stresses over the thick ice would be relevant and the stresses given by equations [16] and [17] would be too large by a factor of 1/A (where A is the compactness). Gray and Morland do take the leads fraction into account; however, as the shear strength of water is much less than that of ice, and if (as Gray and Morland assume) the leads are moving slowly with the ice, then the same depth of water can support far less shear than the ice can. Consequently, the stress applied by the wind to the top of the lead must be about the same as that applied by the bottom of the lead to the ocean below, and there is no net (depth integrated) stress contribution from these two factors.

The suggested new equations are

$$\tau_a = \rho_a c_a A u_G [u_G \cos\theta + k \times u_G \sin\theta] \quad [30]$$

and $$\tau_w = \rho_w c_w A |u_w - u| [(u_w - u) \cos\phi + k \times (u_w - u) \sin\phi] \quad [31]$$

In the constitutive laws of Gray and Morland, the area mean extra stress depends on compactness via the product A f(A) , which scales down the expression for stress in a field of floes with 100% edge contact and 100% ice cover. It accounts for the (linear) decrease in total ice stress per unit mixture area just because there is less ice within which the stress can act, and the (unknown) decrease in ice stress due to reduced floe interactions. The equivalent portion of the Hibler model is the factor exp[-c (1-A)] which attempts to describe the more complicated situation of interactions between 'thick' and 'thin' ice.

5. SUMMARY AND DISCUSSION

The main model features are summarised in the following table:

	Mixed Layer	Lateral Melt	Yield Curve	Ridging
Viscous-plastic (std.) Hibler (1982)	at freezing point	none	elliptical empirical	uniform redistribution
Viscous-plastic (full) Hibler (1980)	coupled with lateral melt	coupled with T_{mix}	elliptical empirical	triangular ridges
Bratchie (1984)	at freezing point	fixed fraction of vertical melt	sinusoidal lens theoretical	triangular ridges
Cavitating fluid Flato & Hibler (1990)	at freezing point	none	none - no shear strength	uniform redistribution
Gray & Morland (1992)	not described	none	none - examine edge interactions	uniform within ridging fraction

All the above tackle the vertical thermodynamics in a similar way, with none of them explicitly describing the snow cover.

Flato and Hibler (1990) point out that 'the lack of shear strength in the cavitating fluid model does affect the details of the thickness and circulation patterns and so [the model is more appropriate for long term, crude resolution climate studies than for the predictions of ice drift and local build up.' The model is relatively inappropriate for FOAM.

The model of Gray and Morland (1992) may eventually warrant further examination. At present, however, there remains a considerable amount of work to be done further development, coding, and sensitivity studies.

Hibler (1980) assumes that the frictional work involved in ridge building is equal to the work done in raising the potential energy of the rubble, as was estimated by Rothcock (1975). Recent numerical studies by Hopkins et al. (1991) suggest that although this may be the case for cylindrical rubble, ridges composed of rectangular blocks use up frictional energy approximately five times as quickly as they create potential energy. Rough theoretical calculations yield even higher estimates for this ratio and sensitivity studies showed it to be strongly dependent on the coefficient of friction between the blocks. In the model of Bratchie (1984), the ratio of frictional to potential energy losses for realistic ice depths varies between 5:1 and 3:2. Until frictional parameterisation is known more precisely, it

seems wise not to include this approach in the sea ice model. Moreover, the initial global sea ice model should be kept relatively simple and refinements made later, as required.

The Bratchie model was designed with the purpose of modelling floe distributions in the marginal ice zone. It is probably more applicable to Antarctic than central Arctic sea ice since the former is a 'loose' pack.

Gray and Morland (1992) point out an inconsistency in the momentum balance of Hibler: the air and wind stresses act on leads as they do on ice - yet the magnitude of the shear stress likely to be produced by this cannot be supported by the thin layer of water moving slowly within the lead - and, more to the point, the momentum balance of Hibler is purely for the ice layer. Also, McPhee (1991) shows that internal waves can make a significant contribution to the water stress term and suggests that their effects be included in future treatments.

The two thickness model of Hibler (1982) is relatively well tested in Arctic and Antarctic (e.g. Hibler and Ackley , 1983) conditions and has been successfuly coupled to an ocean general circulation model. It will now be used to represent sea-ice in FOAM, subject to a likely alteration in the air and wind stress terms.When sufficient information on phenomena such as ridging and floe interaction is available, refinements will be considered. It is also likely that smaller scale sub-models will eventually be created to represent regions of special interest. The form of these models is as yet undecided.

BIBLIOGRAPHY

Anton H. (1984): "Elementary Linear Algebra.", John Wiley and Sons Inc. (4^{th} ed.), 289-290

Bratchie L.L. (1984): "Modelling sea ice floe fields.", Ph.D. Churchill College, Cambridge, in association with the Meteorological Office (U.K.).

Bryan K. (1969): "A numerical method for the study of the circulation of the world's oceans.", J. Comput. Physics, **4**, 347-376.

Bryan K. and Cox. M.D. (1972): "The circulation of the world ocean: a numerical study. Part I, a homogeneous model.", J. Phys. Oceanogr., **2**, 319-335.

Carmack E.C. (1990): "Large-scale physical oceanography of polar oceans.", in Polar Oceanography, Part A - Physical Science, ed. W.O. Smith Jr., Academic Press Inc., 171-222.

Coon M.D. (1980): "A review of AIDJEX modelling.", in Sea Ice Processes and Models, ed. R.S. Pritchard, University of Washington Press, Seattle, 12-27.

Cullen M.J.P. (1991): "The unified forecast/climate model.", Meteorological Office, Short Range Forecasting Division Scientific Paper no. 1.

Flato G.M. and Hibler W.D. III (1990): "On a simple sea-ice dynamics model for climate studies.", Ann. Glaciol., **14**, 72-77.

Gow A.J. and Tucker W.B. III (1990): "Sea ice in the polar regions.", in Polar Oceanography, Part A - Physical Science, ed. W.O. Smith Jr., Academic Press Inc., 47-122.

Gray J.M.N.T and Morland L.W. (1992): "A two-dimensional model for the dynamics of sea ice.", (unpublished to date).

Hibler W.D. III (1979): "A dynamic thermodynamic sea ice model.", J. Phys. Oceanogr., **9**, 815-846.

Hibler W.D. III (1980): "Modelling a variable thickness sea ice cover.", Mon. Wea. Rev., **108**, 1943-1973.

Hibler W.D. III and Ackley S.F. (1983): "Numerical simulation of the Weddel Sea pack ice.", J. Geophys. Res., **88**, 2873-2887.

Hibler W.D. III and Bryan K. (1987): "A diagnostic ice-ocean model.", J. Phys. Oceanogr., **17**, 987-1015.

Hibler W.D. III and Walsh J.E. (1982): "On modelling seasonal and interannual fluctuations of arctic sea ice.", J. Phys. Oceanogr., **12**, 1514-1523.

Maykut G.A. and Untersteiner N. (1971): "Some results from a time-dependent thermodynamic model of sea ice.", J.Geophys. Res., **76** (6), 1550-1575.

Parkinson C.L. and Washington W.M. (1979): "A large scale numerical model of sea ice.", J. Geophys. Res., **84**, 311-337.

Paterson A.R. (1983): "A first course in fluid dynamics.", Cambridge University Press, 99-101.

Riedlinger S.H. and Preller R.H. (1991): "The development of a coupled ice-ocean model for forecasting ice conditions in the arctic.", J. Geophys. Res., **96** (C9), 16955-16977.

Rothcock D.A. (1975): "The energetics of the plastic deformation of pack ice by ridging.", J. Geophys. Res., **80** (33), 4514-4519.

Semtner A.J. (1976): "A model for the thermodynamic growth of sea ice in numerical inves tigations of climate.", J. Phys. Oceanogr., **6**, 379-389.

Thorndike A.S., Rothcock D.A., Maykut G.A., and Colony R. (1975): "The thickness distri bution of sea ice.", J. Geophys. Res., **80** (33), 4501-4513.

Tucker W.B., Gowe A.J., ans Weeks W.F. (1987): "Physical properties of summer sea ice in the Fram Strait.", J. Geophys. Res., **92** (C7), 6787-6803.

Untersteiner N. (1961): "On the mass and heat budget of arctic sea ice.", Arch. Meteorol. Geophys. Bioklimatol., A, **12**, 151-182.

Walsh J.E., Hibler W.D. III, Ross B. (1985):"Numerical simulation of northern hemisphere sea ice variability, 1951-1980", J. Geophys. Res., **90** (C3), 4847-4865.

Washington W.M., Semtner A.J., Parkinson C., and Morrison L. (1976): "On the develop ment of a seasonal change sea-ice model.", J. Phys. Oceanogr., **6**, 679-685.

FIGURES

Fig. 1

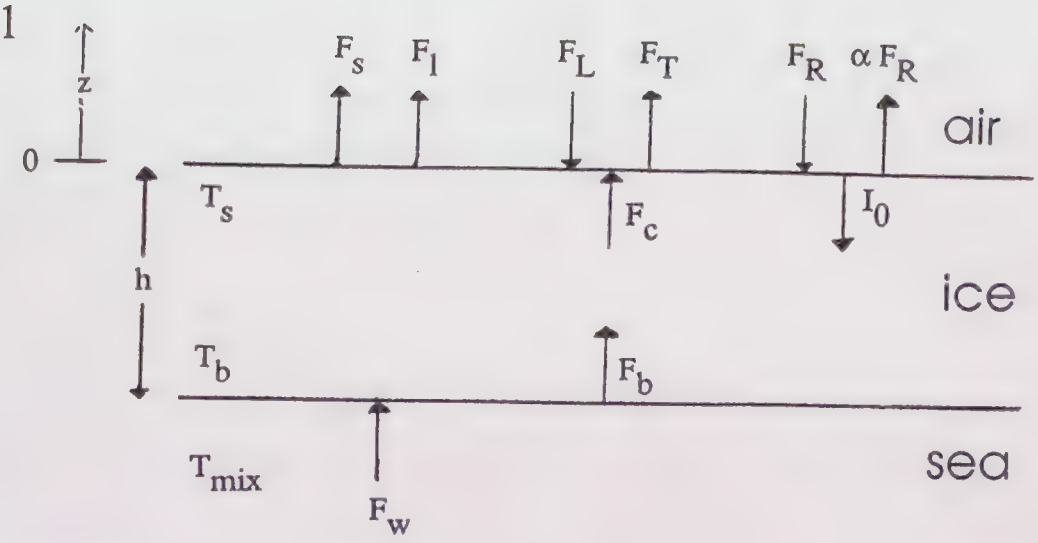

Vertical heat fluxes associated with a layer of sea ice. Variables represent only the magnitude of each flux and the arrows point in the most common direction of heat transport

Fig. 2

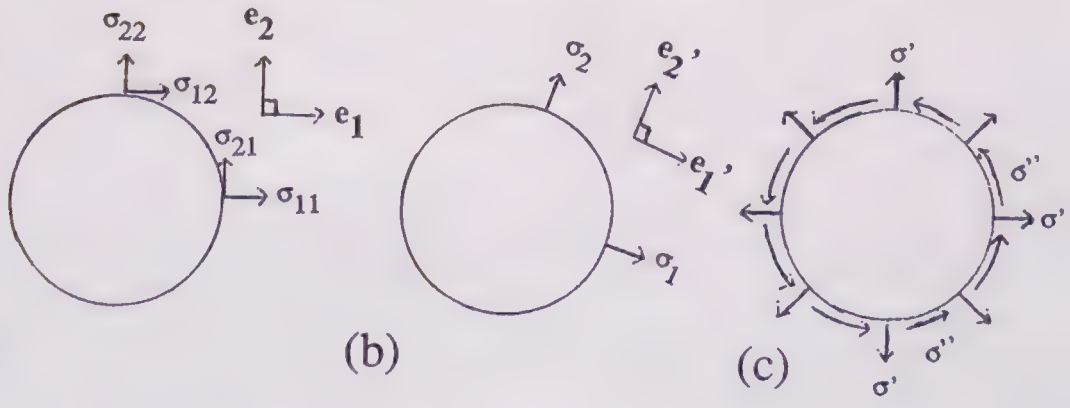

Three ways of representing the stress tensor σ_{ij} at a point embedded in two dimensional space: (a) with respect to the original reference axes e_1 and e_2, (b) as the principal stresses σ_1 and σ_2 acting along the principal axes e_1' and e_2', and (c) as the sum of bulk and shear stresses σ' and σ'' respectively. Each stress component must act on an infinitesimal line segment (as, in two dimensions, a stress is a force per unit length) and there is much scope for confusion when depicting the direction in which each stress component acts when applied to a a particular line segment running through the point in question. Therefore the point is represented as a circle within which the stress tensor is constant and the directions of relevant stress components are given with respect to particular segments of the circle's perimeter.

Fig. 3

Bathymetry and geographic nomenclature for the Arctic Ocean, from Carmack (1990).

Fig. 4

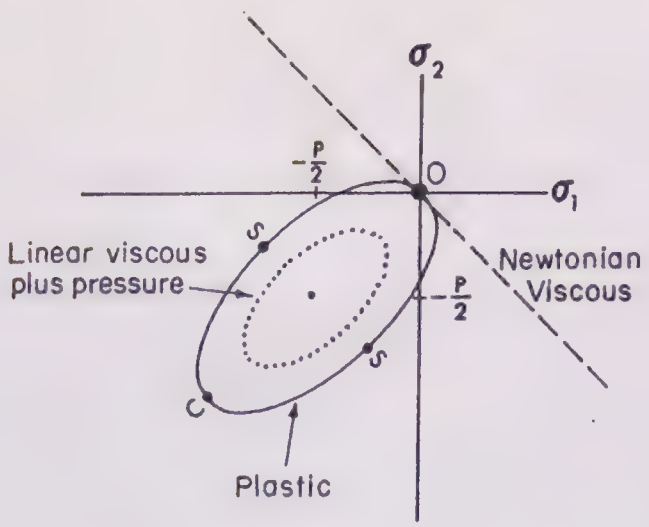

Relationship between the principal components of stress for the viscous-plastic rheology of Hibler (1979). For plastic flow, the stress state lies on the solid yield curve with the location dictated by the ratio of the strain rate principal components. For example, the stress state for pure shearing is located at S , and at C for isotropic compression. For comparison, the stress states for a Newtonian viscous fluid lie on the dashed line. In all cases negative values of σ_1 and σ_2 represent compressive stresses and positive values tensile stresses. (Taken from Hibler, 1979).

Fig. 5

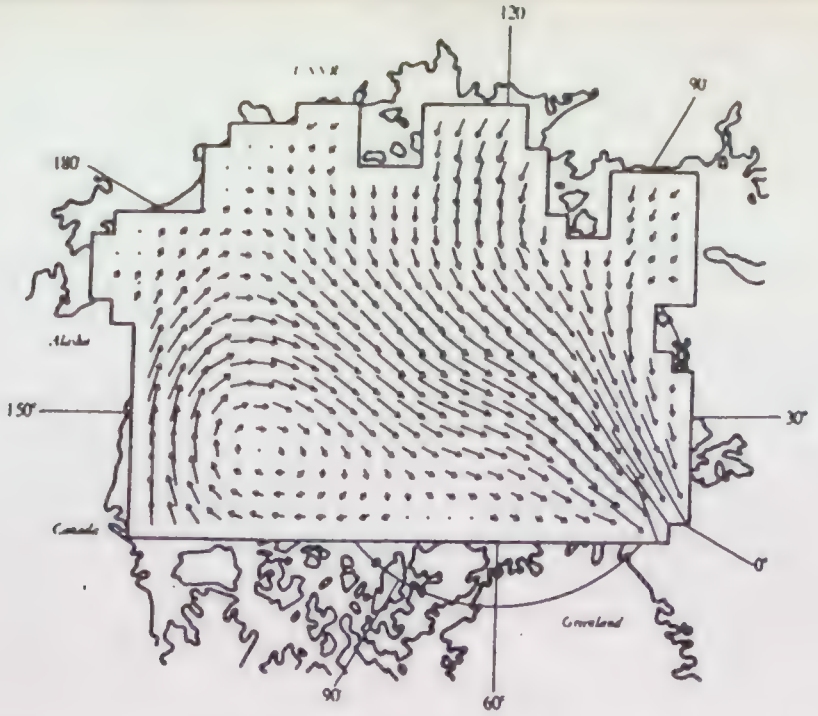

Average annual ice velocity field for the simulation of Hibler (1979). A velocity vector of one grid length represents $0.02ms^{-1}$.

Fig. 6 (a)

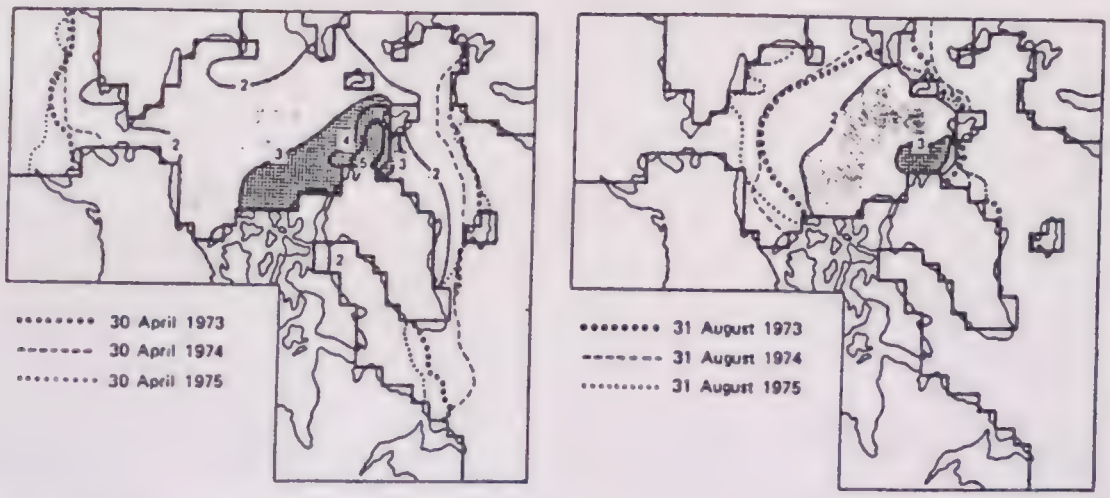

(b)

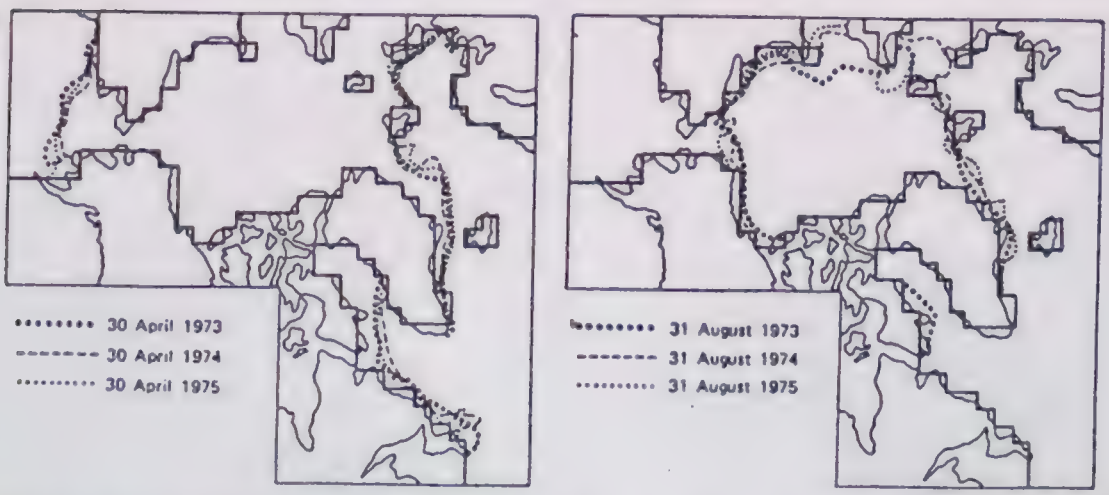

Simulated (a) and observed (b) ice edge at the end of April and August 1973-1975, from Hibler and Walsh (1982). Three year means of simulated ice thicknesses (m) for April and August are also shown in 6a.

Fig. 7 (a)

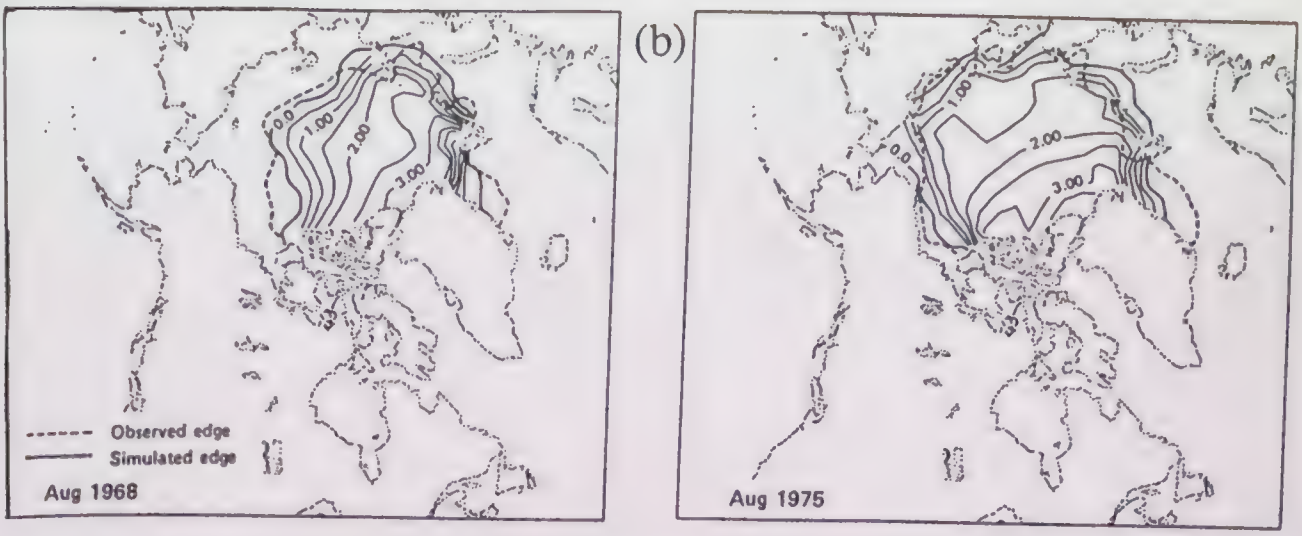

Comparison of simulated and observed ice cover at the end of August 1968 and 1975 from Walsh et al. (1985). Heavy solid lines indicate simulated ice edges and heavy dashed lines indicate observed ice edges. Thin solid lines are contours of simulated ice thickness (m).

Fig. 8 (a)

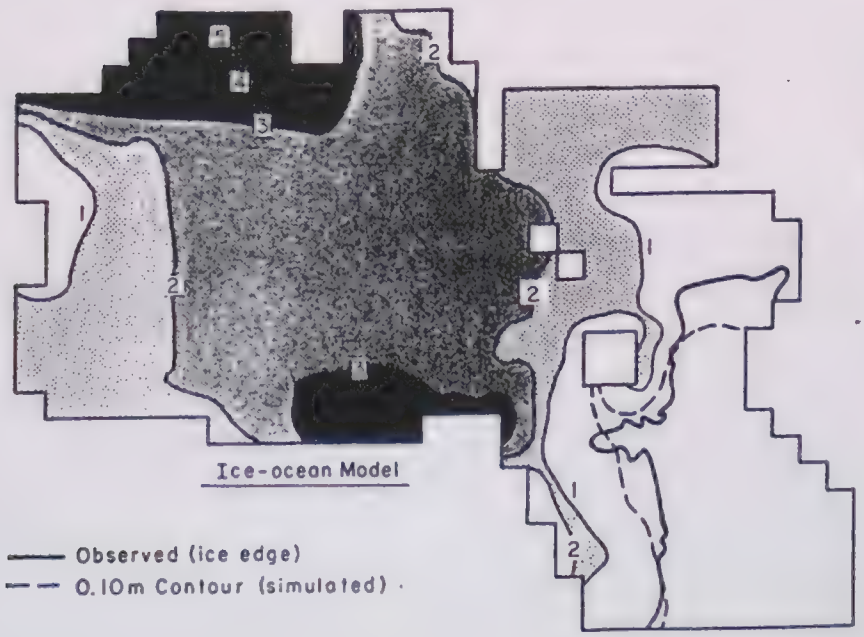

(b)

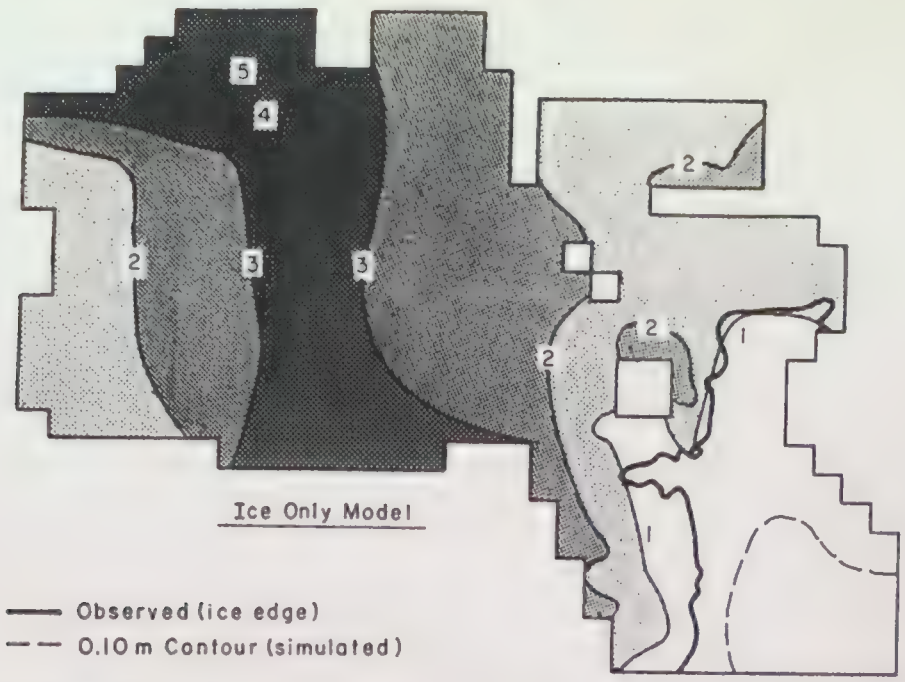

Average February ice thickness contours (m) for (a) the coupled ice-ocean model, and (b) the ice only model; after Hibler and Bryan (1987). Also plotted is the observed ice edge for February 1979 (heavy solid line) and the 0.10m thickness contour (dashed) from the model results.

Fig. 9

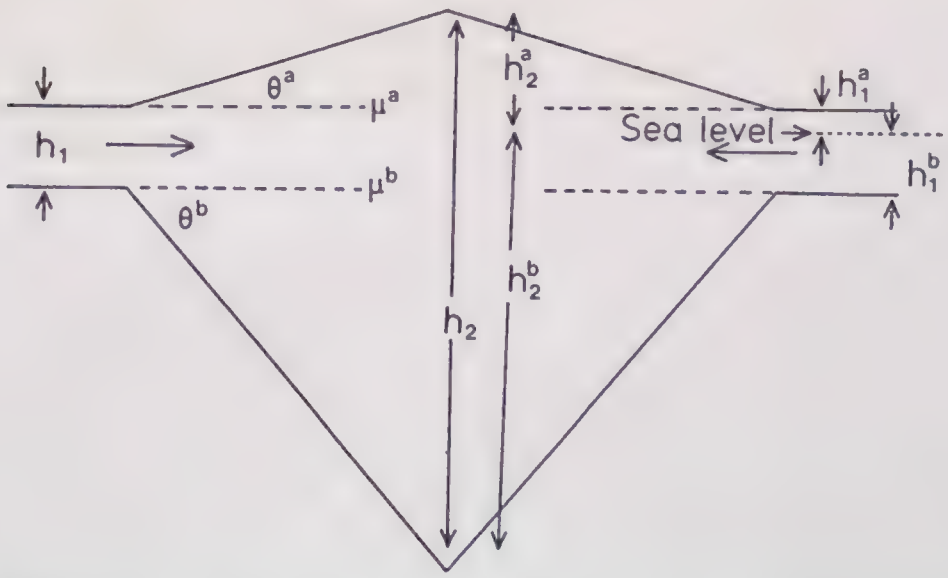

The assumed cross-section of a ridge used in calculating the height of ridges produced (h_2) as a function of the original thickness (h_1). μ^a and μ^b are the coefficients of friction at the top and bottom of the bars of ice and ice rubble (of thickness h_1) that are pushed into the sides of the ridge as it forms (Bratchie, 1984).

Fig. 10

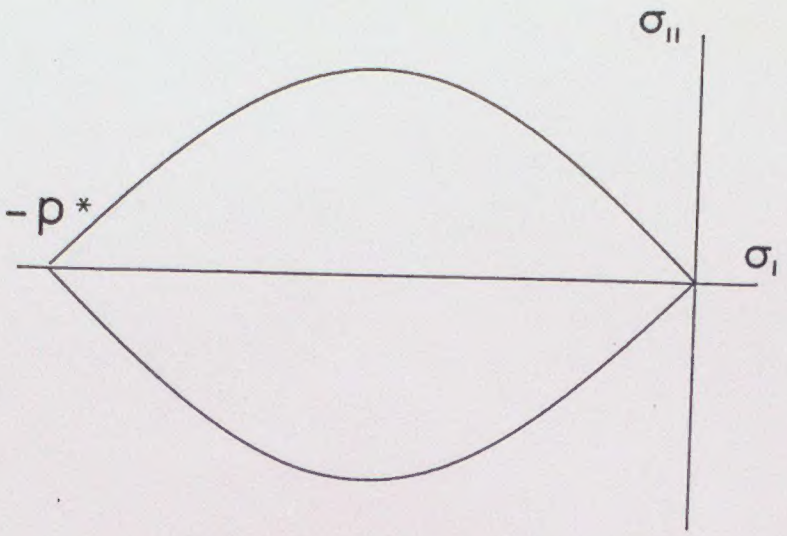

The lens shaped yield curve with bulk and shear stress invariants as the x and y axes respectively - from Bratchie (1984).

Forecasting Research Division Technical Reports

Forecasting Research Division Technical Reports

1.	ON THE TIME SAVING THAT CAN BE ACHIEVED BY THE USE OF AN OPTIMISED COURSE IN AN AREA OF VARIABLE FLOW	R.W. Lunnon A.D. Marklow September 1991
2.	Treatment of bias in satellite sea surface temperature observations	R.S.Bell August 1991
3.	FINITE DIFFERENCE METHODS	M.J.P. Cullen August 1991
4.	Representation and recognition of convective cells using an object-orientated approach	W.H. Hand 30th September 1991
5.	Sea-ice data for the operational global model.	C.P.Jones November 1991.
6.	Tuning and Performance of the Atmospheric Quality Control.	N.B. Ingleby. December 1991.
7.	More satellite sounding data - can we make good use of it?	R.S.Bell January 1992.
8.	WAM/UKMO Wind Wave model Intercomparison Summary Report	Heinz Gunther ECMWF Martin Holt UK Met Office January 1992
9.	Spin up problems of the UKMO Mesoscale Model and moisture nudging experiments	Akihide Segami JMA February 1992
10.	A comparison of 2nd generation and 3rd generation wave model physics	M.W. Holt B.J. Hall February 1992
11.	RETRIEVAL AND ASSIMILATION: SYSTEM CONSIDERATIONS	Andrew C Lorenc March 1992
12.	Detection of Precipitation by Radars in the UK Weather Radar Network	M. Kitchen P.M. Brown April 1992
13.	THE VALUE OF WIND OBSERVATIONS FOR WEATHER FORECASTING AND CLIMATE STUDIES	Andrew C Lorenc April 1992
14.	An investigation into the parameters used in the analysis scheme of the Mesoscale Model	G. Veitch B.J. Wright S.P Ballard May 1992
15.	THE VERIFICATION OF MESOSCALE MODEL FORECASTS OF LIQUID WATER CONTENT USING HELICOPTER REPORTS OVER THE NORTH SEA DURING WINTER 1991	M. Ahmed R.W Lunnon R.J. Graham May 1992

Forecasting Research Division Technical Reports

16.	Simulations of the Diurnal Evolution of Marine Stratocumulus Part I: The sensitivity of the Single Column Version of the Mesoscale Model to Changes in the Turbulence Scheme.	S.D.Jackson S.P. Ballard May 1992
17.	Simulations of the Diurnal Evolution of Marine Stratocumulus Part II: A Comparison of Radiation Schemes Using the Single Column Version of the Mesoscale Model.	S.D.Jackson S.P. Ballard May 1992
18.	Quantifying the low level windshear aviation hazard for the UK: some research proposals	R.J. Graham R.W. Lunnon May 1992
19.	WAM/UKMO Wind Wave model Intercomparison Part 2 Running the UKMO wave model at higher resolution	M.W. Holt April 1992
20.	Sensitivity of Mesoscale Model forecasts of anticyclonic Statocumulus to the specifications of initial conditions and Boundary Layer mixing scheme.	B.J. Wright S.P. Ballard July 1992
21.	Evaluation of diffusion and gravity wave changes in the Global Forecast Model.	F. Rawlins O. Hammon 16 June 1992
22.	Background Errors for the Quality Control and Assimilation of Atmospheric Observations in the Unified Model - the situation in July 1992.	C.A. Parrett July 1992
23.	Estimation of the Mean and Standard Deviation of the Random Component of Data also Containing Non- random Errors.	B.R. Barwell July 1992
24.	Experiments in Nowcasting convective rain using an object- oriented approach.	W.H. Hand 15th August 1992
25.	Gravity Wave Speeds from the Eigenmodes of the Unified Model.	I. Roulstone 28 July 1992
26.	A re-calibration of the Wave Model	M.W. Holt August 1992
27.	Evaluation of Koistinen's method of radar range and bright band correction	A.G. Davies August 1992
28.	A Study of the Boundary Layer in the Mesoscale Unified Model	Graham Veitch August 21,1992
29.	Profiles of wind using time-sequences of absorption channel imagery from geostationary satellites: proof of concept using synthetic radiances	R.W.Lunnon September 1992
30.	AN EMPIRICAL INVESTIGATION OF THE "WATER VAPOUR TEMPERATURE LAPSE-RATE FEEDBACK" TO THE GREENHOUSE EFFECT	K.F.A. Smith R.J. Allam J.S.Foot September 1992
31.	Observation needs for operational ocean modelling	S.J. Foreman September 1992

Forecasting Research Division Technical Reports

32.	Bright band correlations for layered precipitation; the comparison of Chilbolton radar data and Hardaker model output.	A.G. Davies November 1992
33.	Progress and performance of the operational mesoscale model	S.P. Ballard
34.	Assessment of the bias of significant wave height in the Met.Office global wave model	S.J. Foreman M.W. Holt S. Kelsall
35.	STUDY OF CIRRUS CLOUD WINDS: ANALYSIS OF I.C.E DATA FINAL REPORT FOR EUMETSAT CONTRACT ITT 91/16	R.W. Lunnon D.A. Lowe J.A. Barnes I. Dharssi December 1992
36.	Revisions to the operational data assimilation-Nov.92	R.S. Bell January 1993
37.	A comparison of wind observations from a flight of the DRA(B)BAC 1-11 research aircraft over Hemsby, 11 June 1991, with observations from the Hemsby radiosonde	R.J. Graham January 1993
38.	The Moisture Observation Pre-processing System	B.J. Wright January 1993
39.	Performance of the data assimilation scheme in the operational trial of the new mesoscale model.	B. Macpherson B.J. Wright A.J. Maycock January 1993
40.	Development and performance of the new mesoscale model.	S.P. Ballard B. Robinson January 1993
41.	A PRELIMINARY ASSESSMENT OF OCEAN SURFACE FLUXES FROM UNIFIED MODEL FORECASTS	J.O.S. Alves S.J.Foreman M.W. Holt S. Kelsall S.J.Nightingale January 1993
42.	Some notes on primitive and quasi-equilibrium equations with a hybrid vertical coordinate and remarks on Hamiltonian structure.	I.Roulstone 23rd March 1993
43.	Development of the surface data assimilation scheme for the new mesoscale model	A.J. Maycock April 1993
44.	A REVIEW OF SEA ICE MODELS FOR USE IN FOAM	C.G. Sherlock April 1993